# Method for determination of the volume of material ejected as molten droplets during visible nanosecond ablation

Jennifer M. Fishburn, Michael J. Withford, David W. Coutts, and James A. Piper

A novel method is presented for determining the volume of molten material ejected from a substrate as a result of visible pulsed-laser ablation. A 100-μm-wide pulsed-laser light sheet ($\tau \sim 5$ ns, $\lambda = 532$ nm) was used in conjunction with a CCD camera to provide high-speed cross-sectional images of single-pulse ablation of aluminum with a visible nanosecond laser source. Computational analysis of the two-dimensional gray-scale images was used to determine the total volume of material ejected from the substrate in the form of molten droplets. Ablation with dual-wavelength (511- and 578-nm) pulses of 30-ns duration was characterized under various fluence conditions (0–25 J $cm^{-2}$), allowing a quantitative threshold for explosive melt ejection in aluminum to be established at ~10 J $cm^{-2}$. The temporal evolution of the ejected material showed that, for an incident fluence of ~40 J $cm^{-2}$, molten-droplet ejection commenced at ~400 ns and ceased after ~2 μs. 

*OCIS codes:* 100.2960, 140.3390, 350.3390.

## 1. Introduction

The development of a comprehensive theoretical framework for nanosecond pulsed-laser ablation of metals is crucial to the optimization of laser micromachining parameters for a variety of important industrial processes. However, such development is impeded by the lack of quantitative characterization of a high-fluence (≥10-J $cm^{-2}$) ablation mechanism whereby molten material droplets are ejected from the samples surface. This mechanism, termed here explosive melt ejection, is generally associated with phase explosion[1] and is energetically efficient because significant material is removed at energies less than the latent heat of vaporization. In the past, fluence thresholds and the total volumes of explosive melt ejection were determined through measurements of the weight change of the substrate used to collect the molten ejecta.[2] However, several effects reduced the capture efficiency, leaving a significant fraction of ejected material unaccounted for. Alternatively, explosive-melt ejection could be studied indirectly through estimates of crater depth and volume derived from profilometry of the ablation pit for appropriate laser fluence regimes.[3] The latter method suffered seriously from an inability to distinguish among the several ablation mechanisms (vaporization, melt displacement, explosive melt ejection). Neither approach revealed any information about the dynamics of explosive melt ejection. In the present paper we present a new method for characterizing explosive melt ejection based on use of high-speed image analysis. As well as clearly distinguishing explosive melt ejection from other ablation mechanisms and permitting the determination of absolute ejected volumes, the method gives substantial information about the dynamics of explosive melt ejection.

## 2. Experimental Details

The laser ablation source for all experiments was a copper-laser master oscillator–power amplifier system providing single, 30-ns pulses at combined wavelengths of 511 and 578 nm with pulse energies of as much as 1.3 mJ. A multimode optical fiber was placed between the oscillator and the double-pass amplifier, and the output was focused to a spot radius of 37 μm with a top-hat irradiance profile on the surface of an aluminum (99.99%) substrate. The optical delivery system that is required for this output

When this research was performed the authors were with the Centre for Lasers and Applications, Macquarie University, Sydney NSW 2109, Australia. (e-mail for M. J. Withford, withford@ics.mq.edu.au). D. W. Coutts is now with Clarendon Laboratories, University of Oxford, Oxford, United Kingdom.

Received 4 May 2004; accepted 26 July 2004.
0003-6935/04/356473-04$15.00/0

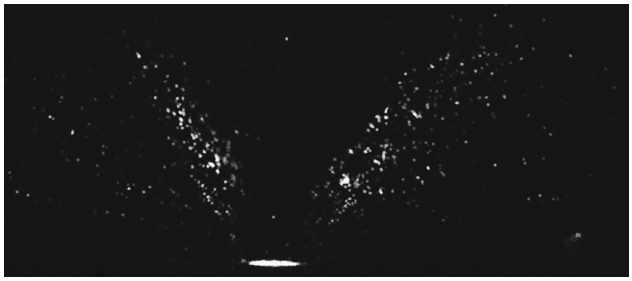

Fig. 1. Typical gray-scale image obtained during ablation with a visible nanosecond laser pulse.

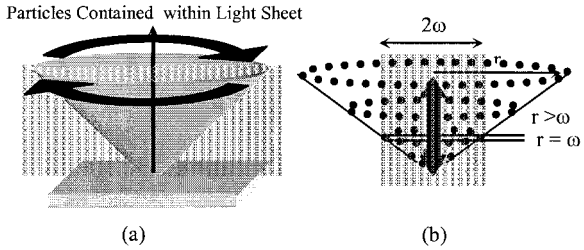


Fig. 2. (a) Three-dimensional rotational analysis of the droplets contained within each image (front view). (b) Adjustment for the finite width of the light sheet (side view).

is fully described in Ref. 4. A 5-ns, frequency-doubled (532-nm) Nd:YAG light sheet ~100 μm thick and ~7 mm wide was used to illuminate a cross-sectional slice of the molten droplets that were ejected by ablation. An image of the illuminated droplets was captured by a high-speed CCD camera and magnification system. The resolution of this system was 2.25 μm. A notch filter at 532 nm placed between the camera and the ablation site allowed images to be captured during the 511–578-nm ablation pulse with no damage to the camera. Images from the camera were taken in a gray-scale format, with each pixel value (0–255) representing an intensity of detected light. A typical image is given in Fig. 1. Each image was processed by National Instruments software that comprised a customized image analysis module (IMAQ) in a LabVIEW environment, yielding the dimensions and position of each particle.

Closer analysis of the images shows that the majority of particles ejected from the sample are in the form of elliptical or spherical droplets. However, deviations from these generic shapes do occur when two particles overlap and are seen in the image as one larger, misshapen particle. (With the sparse nature of particles illuminated by the light sheet in the current analysis this occurs only rarely.) The analysis consisted of using the individual particle areas and perimeters to approximate corresponding major and minor elliptical axes ($a$ and $b$, respectively) for each of the particles. This method, which was correct for both spherical and elliptical particles, was also able to offset the effect of overlapping particles, as the single particle identified by the IMAQ module had an increased ratio of perimeter to cross-sectional area (this advantageously results in overestimation of the major and minor axis values attributed to the particle). Assuming a symmetrical mass distribution about the major axis (which was in the direction of travel), we used these axis values to calculate the total volume, $V = 4\pi ab^2$, of each particle illuminated by the light sheet. Indeed, simulations of several artificial particles of known size and various amounts of overlap showed an error of <5% for overlaps of as much as 50%. This is an acceptable margin compared with the ~10% error that is typically associated with profilometric analysis techniques. Of course, this issue would be a much greater concern for analysis of higher concentrations of particles; in such cases the light sheet's thickness would need to be decreased to permit sufficiently accurate analysis. During extrapolation from the individual particle data to determine the total volume of material ejected from the sample, a conical three-dimensional distribution of ejecta symmetric about a central axis was assumed [see Fig. 2(a)]. It is important to note that, owing to the finite width of the light sheet, the angular fraction of the particles illuminated by the light sheet closer to the sample was larger than that for particles observed farther away [Fig. 2(b)]. To compensate, the fraction of particles contained within the light sheet of width 2ω was determined for each particle position, $r$. It was assumed that a similar volume of material existed within each 2ω slice about a rotation of π rad about the central axis as the light sheet illuminated both sides of the ejected droplets. The total volume of material removed from the sample in the form of melted droplets could then be calculated. A critical component in the analysis of these gray-scale images was the specification of a threshold pixel value to define the boundaries of each particle. Figure 3 shows the dependence of the estimated volume on the pixel value for a single image processed at various pixel thresholds.

It is clear from the range of volumes that signifi-

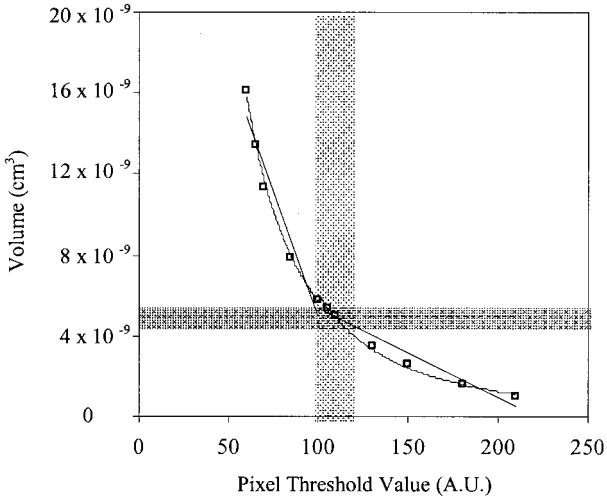


Fig. 3. Volumes obtained from a single image as a function of pixel threshold. (Shaded regions demarcate boundaries of reasonable pixel values as determined by errors in the $x$ and $y$ axes.)

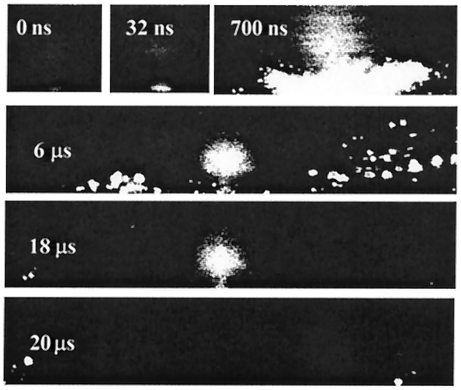


Fig. 4. Temporal evolution, showing plasma formation.

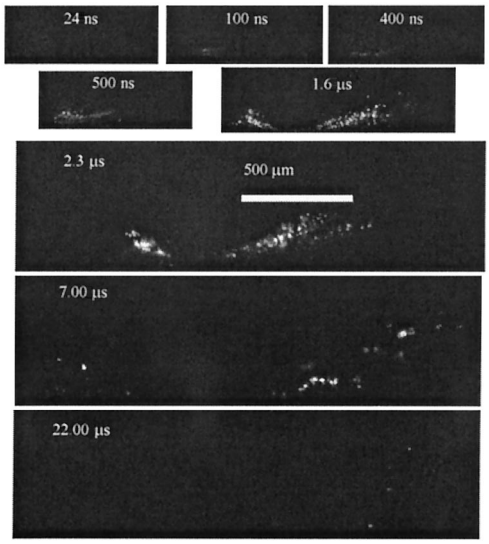


Fig. 5. Images showing the temporal evolution of ejected material as a result of a single ~40-J $cm^{-2}$, 30-ns pulse.

cant error may be introduced at this step. The vertical shaded region in Fig. 3 represents the range of plausible pixel values that were identified by examination of the image. Processing at low pixel values (100) caused the halo of light scattered from the particles to be interpreted as valid matter, making two close particles indistinguishable and thereby overestimating the actual amount of material. However, when the images were filtered with a high threshold value (120), valid particles were disregarded, resulting in an overall underestimate. A pixel threshold value of 110 that lay midway between these two boundaries was chosen; a ±10% error in relating to the range of possible pixel thresholds was assumed. Alternatively, the volume as calculated from profilometric measurements could be used for calibrating the image analysis data. The crater volume calculated from profilometry, with an uncertainty of ±10%, is represented by the horizontal shaded region in Fig. 3. In practice, the most appropriate threshold should be set by use of both the image resolution criteria discussed above and profilometric calibration for a fluence for which melt ejection is dominant. Note that, for a given experimental setup, setting the pixel threshold is required only once.

### 3. Experimental Results and Discussion

The images in Fig. 4 show all pixel information above the noise level of the camera (pixel value, ~26). They show the temporal evolution of ejected material that results from a single ~40-J $cm^{-2}$, 30-ns pulse. The times given mark the delay between the peak of the ablative laser pulse and the image. The formation of a region of emission in the area directly above the ablation site is evident. This emission, beginning within the first 100 ns and remaining static in space until its disappearance ~20 μs later, is identified as a plasma ball. The pixel information contained within this area is thus excluded from any subsequent mass or volume calculations from the images. A subset of the unprocessed images used for studying the temporal evolution of the volumetric removal of material is provided in Fig. 5. Ejection of particulate matter at an angle of <20° to the surface is observed to begin approximately 400–500 ns after the peak of the irradiation pulse. After 2–3 μs, there is a cessation in this material ejection, with no new material observed to be ejected after this time. Note that at this time all material lies within the field of view of the camera. For this reason, all subsequent images in this study were taken at a time delay of ~2.7 μs. A quantitative analysis of the volumes of melt ejecta contained within each image (based on the threshold pixel value of 110) is presented in Fig. 6. The volume of material ejected is observed to increase linearly with time from 400 ns after the ablative pulse to ~2 μs later. This increase is then followed by decreases in ejecta volumes observed at later times, consistent with droplets' moving out of the light sheet's field of view. As confirmation of the self-consistency of this technique, the maximum ejected volume of approximately $5–6 \times 10^{-9}$ $cm^3$ that occurs at a delay time of 2–3 μs corresponds well to

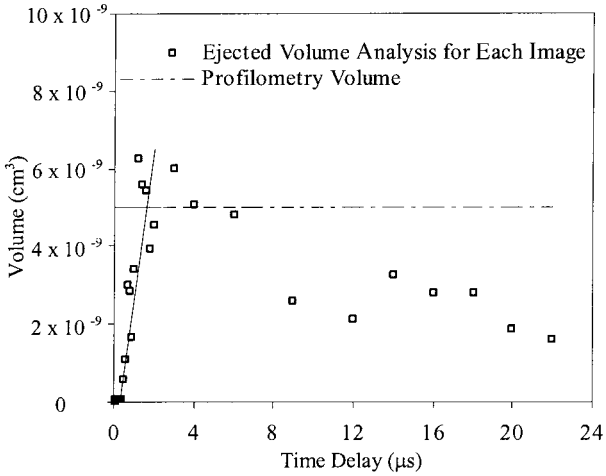


Fig. 6. Volume of melt ejecta contained within images taken at increasing time delays after ablation with a single ~40-J $cm^{-2}$, 30-ns pulse.

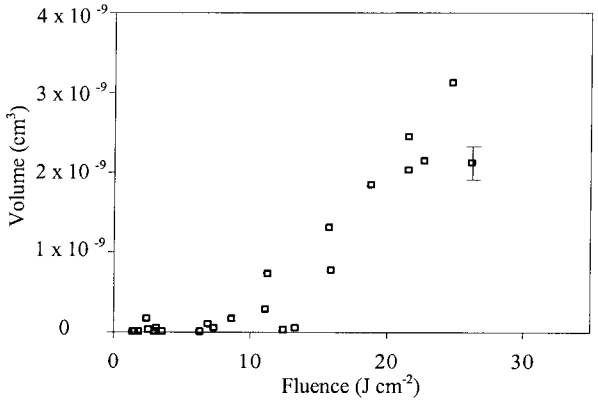


Fig. 7. Volume of material ejected as a result of ablation with increasing fluence (spot radius, ~37 μm).

the total crater volume at a similar fluence of $\sim 5 \times 10^{-9}$ cm$^3$ as measured by profilometry (also shown in Fig. 6).

Data showing the volume of explosively ejected material measured by way of image analysis as a function of single-pulse fluence are given in Figure 7. The data indicate that the fluence threshold for explosive melt ejection lies in the approximate range 8–10 J cm$^{-2}$ for visible nanosecond ablation of aluminum. This threshold fluence value is in good agreement with other investigations[5] for which the onset of explosive melt ejection was estimated to be 6–8 J/cm$^2$ for aluminum samples ablated with a laser source of similar parameters ($\tau_p \sim 6$ ns, $\lambda = 532$ nm). In the latter case the threshold onset for explosive behavior was based on observations of marked increases in the intensity of light in images of the ablation plume coupled with a significant increase in the weight loss of the sample as fluence was increased. Whereas these measurement techniques may indicate a change in ablation mechanism, they do not permit one to determine the contribution of melt ejection to the overall material removal. In contrast, the image analysis technique presented here permits a better determination of the volume of material removed by explosive melt ejection as distinct from vaporization or melt displacement as well as identifying the onset threshold fluence of the melt ejection mechanism. In addition, the angle of ejection and velocity for the melt ejecta can be directly determined from the images. We intend to use this angular information in conjunction with a volume–mass analysis of the melt ejecta to isolate the contribution of explosive melt ejection to the overall recoil momentum experienced by the sample as a result of ablation.

## 4. Conclusions

Computational analysis of high-speed images is used to characterize quantitatively the volume of molten droplets ejected from an aluminum substrate as a result of ablation with a single nanosecond laser pulse. Such *in situ* investigation of the spatiotemporal characteristics and absolute ejected volumes of material removal owing to explosive melt ejection can complement and at times replace conventional material analysis techniques such as profilometry of the ablation crater. Investigations during a single ~40-J cm$^{-2}$, 30-ns pulse showed that the material removal, with an acute angle (<20°) to the surface of the sample, began at ~400 ns and ended at ~2 μs. Under conditions of increasing fluence, a sudden increase in the volume of ejected particles was observed at ~10 J cm$^{-2}$, marking the onset of explosive melt ejection.

We gratefully acknowledge the invaluable contribution of Adam Wybrew and Oxford Lasers, Inc., in providing the high-speed imaging laser system and Clarendon Laboratory, Oxford University, for their kind support, and the generous financial assistance of the Australian Research Council.

## References

1. R. Kelly and A. Miotello, "Comments on explosive mechanisms of laser sputtering," Appl. Surf. Sci. **96–98,** 205–215 (1996).
2. P. Solana, P. Kapadia, J. Dowden, W. S. O. Rodden, S. S. Kudesia, D. P. Hand, and J. D. C. Jones, "Time dependent ablation and liquid ejection processes during the laser drilling of metals," Opt. Commun. **191,** 1–2 (2001).
3. J. H. Yoo, O. V. Borisov, X. Mao, and R. E. Russo, "Existence of phase explosion during laser ablation and its effects on inductively coupled plasma-mass spectroscopy," Anal. Chem, **73,** 2288–2293 (2001).
4. D. W. Coutts, "Double-pass copper vapor laser master-oscillator power-amplifier systems: generation of flat-top focused beams for fiber coupling and percussion drilling," IEEE J. Quantum Electron. **38,** 1217–1224 (2002).
5. A. Mele, A. G. Guidoni, R. Kelly, C. Flamini, and S. Orlando, "Laser ablation of metals: analysis of surface-heating and plume-expansion experiments," Appl. Surf. Sci. **109–110,** 584–590 (1997).